STUDY OF AERODYNAMIC NOISE OF PROPELLER CONSIDERING THE INFLUENCE OF BOUNDARY SURFACE USING CFD METHOD

Thanh Dong Pham[1,*], Quang Quyen Le[1], Ngoc Thanh Dang[1], Quoc Tru Vu[1]

[1]*Faculty of Aerospace Engineering, Le Quy Don Technical University*

Abstract

This article focuses on the aerodynamic and acoustic characteristics of both an isolated propeller model and a propeller - boundary surface model. The study uses the Reynolds-averaged Navier-Stokes (RANS) method combined with Computational Fluid Dynamics techniques to analyze the flow field and wake flow behind the propeller and to determine its basic aerodynamic coefficients. The pressure on the surface of the propeller and boundary surface is used as input for the noise calculations. An acoustic analogy method, based on the Farassat 1A formulation derived from the Ffowcs Williams-Hawkings (FW-H) equation, is employed to calculate the propagation of noise from the surfaces of the propeller and boundary surface to designated positions (microphones). The research results lead to some significant conclusions drawn by the authors.

Keywords: *Propeller; aerodynamic characteristics; acoustic characteristics; Farassat 1A*.

1. Introduction

Awareness of the adverse effects of noise is increasing in modern society, leading to more and more scientific research focusing on analyzing and seeking solutions to reduce noise [1-3]. Propeller noise is a branch of aeroacoustics, related to the sound generated by aerodynamic forces or unsteady turbulent motions of the airflow. On the other hand, propellers are widely used in most Unmanned Aerial Systems (UAS) of various sizes [4]. The efficiency of UAS operations, meeting mission requirements, heavily depends on the aerodynamic and acoustic characteristics of the propellers during takeoff and landing phases. This is because, when operating very close to the ground or boundary surfaces, UAS create significant aerodynamic disturbances, often referred to as "Ground Effect" [5, 6]. Operating within the Ground Effect can lead to changes in aeroacoustics and increased noise levels, along with changes in stability and flight control requirements. Therefore, studying the aerodynamic and aeroacoustic characteristics during takeoff and landing, as well as the interaction of propellers with boundary surfaces, is crucial. However, currently, there are not many published studies on the acoustic

[*] Corresponding author, email: pham.thanh-dong@lqdtu.edu.vn
DOI: 10.56651/lqdtu.jst.v19.n03.844

characteristics of propellers under these conditions. Furthermore, knowledge about potential noise-reduction strategies for both propellers and boundary surfaces for propeller design, runway surface design, and noise-reducing materials is still very limited.

Many methods for studying the aerodynamic noise of propellers have been developed over the years [7]. However, the most comprehensive and commonly used in most aeroacoustic research is the FW-H equation, published by Ffowcs Williams and Hawkings in 1969, which clearly explains the formation and propagation of sound caused by any rigid surface moving in space [7-10]. The outstanding advantage of the FW-H equation is its various solutions, such as the Farassat 1 and 1A formulations [7, 8], and the 1C formulation by Najafi-Yazdi [9], each of which can be used to solve many specific problems. Currently, noise prediction and acoustic design of propellers mostly rely on the solution of the FW-H equation [10]. In terms of approach, aside from a few studies that have independently developed low-cost computational tools to predict the characteristics of propellers both aerodynamically [11, 12] and aeroacoustically [13], numerical simulation methods and experimental methods are widely used by many scientists today [14, 15]. In this article, the authors aim to use the Computational Fluid Dynamics (CFD) simulation method on Ansys Fluent software to study and determine the aerodynamic and acoustic characteristics of a specific propeller considering the influence of the boundary surface. The research in this article includes two processes: determining the aerodynamic characteristics of the propeller under conditions affected by the boundary surface (ground effect) and calculating sound radiation at desired receiving points by setting the surface pressure distribution of the propeller and boundary surface as the sound source. This approach has been widely applied and published in many studies in various fields [16-20].

2. Simulation model construction

2.1. Governing equations

Navier-Stokes equations: The flow field of the propeller can be assumed to be quasi-steady. Therefore, based on the k-omega turbulence model, the RANS method can be used to determine the average information of the flow field [16-18]. The Navier-Stokes equation in a rotating coordinate system is used below:

$$\frac{\partial}{\partial t}\iiint_V \boldsymbol{W} dV + \iint_{\partial V} \left[F\left(\boldsymbol{W}\right) - G\left(\boldsymbol{W}\right) \right] \boldsymbol{n} dS = \iiint_V \boldsymbol{Q} dV \tag{1}$$

where $\boldsymbol{n}$ is normal vector, $\boldsymbol{Q}$ is additional part causing by rotation, $\boldsymbol{W} = \left[\rho, \rho u, \rho v, \rho w, \rho E\right]^T$, u, v, w are velocity components of fluid, ρ is density of the fluid, E is internal energy of unit fluid, $F\left(\boldsymbol{W}\right), G\left(\boldsymbol{W}\right)$ are viscous flux and inviscid flux, respectively.

Ffowcs Williams-Hawkings Equation and Farassat 1 and 1A Formulas: In 1969, Williams Ffowcs and Hawkings [10] used generalized function theory to derive the sound equation of any rigid surface moving in a static fluid medium, known as the famous FW-H equation. From the late 1970s to the early 1980s, Farassat published the renowned Farassat 1 and Farassat 1A formulas [7, 8] based on the integral of the Green Function and the transformation between spatial and time derivatives. These formulas are solutions to the time-domain integral expressions for thickness noise (TN) and loading noise (LN) of the FW-H equation. The Farassat 1A formula is expressed as below:

$$p'(x,t) = p'_T(x,t) + p'_L(x,t) \tag{2}$$

where $p'(x,t)$ is the total acoustic pressure at observers; $p'_T(x,t)$ and $p'_L(x,t)$ are the pressure causing thickness noise and loading noise, respectively, and can be written as:

$$\begin{aligned} p'_T(x,t) = {} & \frac{1}{4\pi}\int_{f=0}\left[\frac{Q_j n_j}{R^*(1-M_R)}\right]_{ret} dS - \frac{1}{4\pi}M_0\int_{f=0}\left[\frac{\tilde{R}_1 Q_j n_j}{R^*(1-M_R)}\right]_{ret} dS - \\ & - \frac{1}{4\pi}U_0\int_{f=0}\left[\frac{\tilde{R}_1^* Q_j n_j}{R^{*2}(1-M_R)}\right]_{ret} dS \end{aligned} \tag{3}$$

$$p'_L(x,t) = \frac{1}{4\pi c}\int_{f=0}\left[\frac{L_{ij} n_j \tilde{R}_i}{R^*(1-M_R)}\right]_{ret} dS + \frac{1}{4\pi}\int_{f=0}\left[\frac{L_{ij} n_j \tilde{R}_i^*}{R^{*2}(1-M_R)}\right]_{ret} dS \tag{4}$$

Here $\tau = t - \frac{R}{c} = t - \frac{|\boldsymbol{x}-\boldsymbol{y}|}{c}$; $M_R = \frac{1}{c}v_i\tilde{R}_i$; $Q_j = \rho\left(u_j + U_{0j} - v_j\right) + \rho_0(v_j - U_{0j})$; $L_{ij} = \rho u_j\left(u_j + U_{0j} - v_j\right) + P_{ij}$; $P_{ij} = (p - p_0)\delta_{ij} - \sigma_{ij}$ with p is the pressure at source points; c is the speed of sound; ρ_0 is the airflow density; t is the time at observers; τ is the retarded time when the noise is emitted from the source to the observer; $R = |\boldsymbol{x} - \boldsymbol{y}|$ is the distance between the observer and the source, $\boldsymbol{x}$ is the observer position vector, $\boldsymbol{y}$ is the source position vector. $f = 0$ is a function describing the blade surface (source surface);

From the acoustic pressure spectrum data obtained using formulas (2), (3), and (4), the overall sound pressure level (OASPL) at a specific measurement location can be determined. OASPL is a single numerical value that describes the noise source and is defined as the average of all individual sound pressure levels at the frequencies emitted by the noise source. OASPL can be determined using the following expression:

$$\mathrm{OASPL} = 10 \cdot \log_{10}\left[\sum_{i=1}^{n} 10^{\frac{\mathrm{SPL}_i}{10}}\right] = 10 \cdot \log_{10}\left[10^{\frac{\mathrm{SPL}_1}{10}} + 10^{\frac{\mathrm{SPL}_2}{10}} + \ldots + 10^{\frac{\mathrm{SPL}_n}{10}}\right] \quad (5)$$

where SPL_1, SPL_2,…, SPL_n are sound pressure levels at different frequencies, dB.

2.2. Numerical simulation

The 3D propeller model was constructed using the Inventor graphics software with the geometric dimensions shown in Tab. 1 and Fig. 1. The 3D propeller model consists of 2 blades, as illustrated in Fig. 2.

Tab. 1. Geometrical data of propeller

Parameters	**Measurements**
Diameter *D* (mm)	150
Chord width (mm)	11
Pitch angle (°)	35
Number of blades *n*	2
Angular speed Ω (rpm)	5000, 6000, 7000

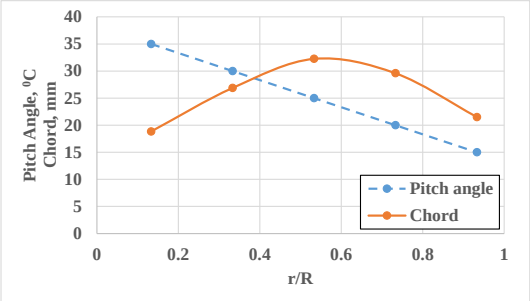

Fig. 1. Geometrical parameters of propeller blade.

The boundary surface is simulated as a thin plate with dimensions of $10R \times 10R$ (where R is the radius of the propeller blade), positioned below the rotor at a distance h. In this simulation model, the distance h is set to values of $0.5R$, $1.0R$, and $1.5R$ (Fig. 2). To measure acoustic data, the authors placed microphones at coordinates mic 1 (1.12, 1.34, 0), mic 2 (1.75, 0, 0), and mic 3 (0.877, -1.5, 0). The microphones are positioned on a circle with a radius of $14R$ from the propeller center, forming angles of 40°, 90°, and 150° with the vertical axis (Fig. 3). Regarding flight mode, this paper focuses on studying the aerodynamic and acoustic characteristics of the propeller in hover mode, which is the basic operational mode during takeoff and landing for small helicopters and rotor-based UAVs.

Using the RANS method combined with CFD techniques integrated within the Ansys Fluent software, the authors proceeded to mesh the survey model, select the viscosity model, set boundary conditions, etc., following steps similar to those in the study [21]. The size of the computational domain (static domain) for the aeroacoustic model Propeller - Boundary surface (Pro - BF) is shown in Fig. 3.

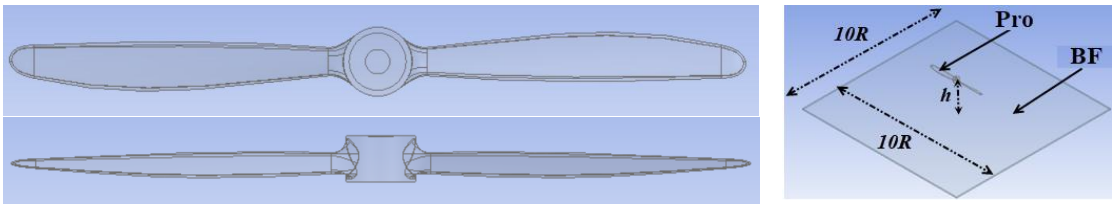

a) b)

Fig. 2. 3D model of propeller (a) and boundary surface (b).

The mesh density was concentrated around the propeller blade and the rotating region, with the boundary layer mesh around the propeller blade consisting of 5 layers with a growth rate of 1.2 (Fig. 4).

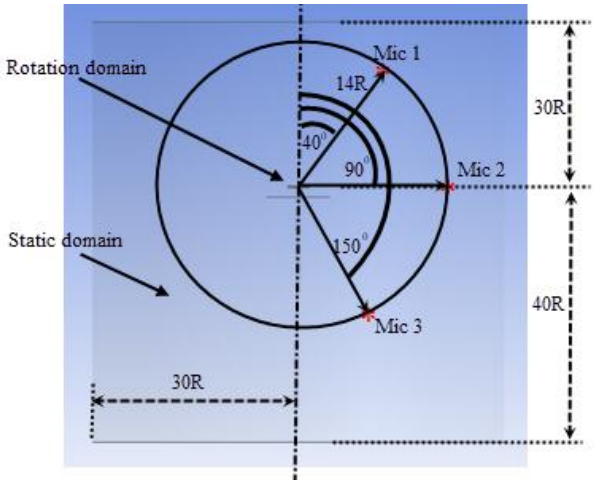

Fig. 3. Microphone positions for measuring aerodynamic noise characteristics.

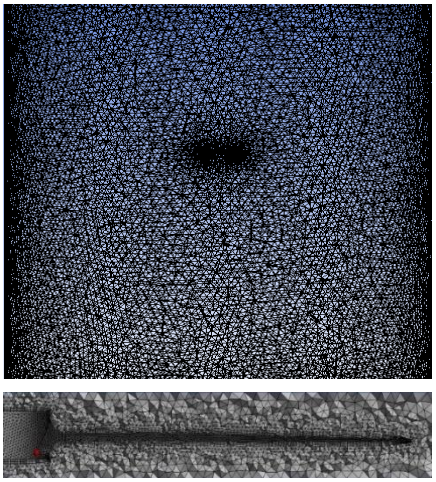

Fig. 4. Grid of domains and propeller.

Simulations were conducted for the propeller model in hovering mode based on the RANS equations with the k-omega SST turbulence model, at an angular velocity of 5000 rpm. Boundary conditions were set for unsteady, compressible flow following the ideal gas law. The boundary condition for the inlet flow was set as Pressure_inlet, and for the outlet flow as Pressure_outlet with values equal to ambient pressure; the wall flow had a velocity of 0. To study the sensitivity of the mesh to the calculation results, the authors determined the thrust coefficient and the torque coefficient of the independent rotor in the case of hovering flight, the rotation speed is 5000 rpm with 3 different mesh sizes of 863000, 1031441 and 1561441 elements, respectively. The calculation data are shown in Tab. 2. The data show that 1031441 grid cells are sufficient to meet the

requirements of the blade calculation accuracy. In this paper, the most suitable grid with 1031441 grid cells was selected for further calculation study.

To validate the computational model, the authors used a propeller model with geometric and kinematic parameters that matched the experimental model from R. Stepanov [22] as a calculation example (Tab. 3). The boundary conditions and viscous models were set as previously described, with the computational grid containing 1.74×10^6 elements [21]. The comparison results shown in Fig. 5 indicate good agreement between the simulation data from the authors' model and the experimental results from R. Stepanov [22]. This demonstrates the reliability of the simulation model presented in this study.

Tab. 2. Aerodynamic coefficients of propeller with different mesh density

Density	**Total cells**	**Thrust (N)**	**Thrust error (%)**	**Torque (N.m)**	**Torque error (%)**
Coarse	863000	2.9	15.69	0.075	3.84
Medium	1031441	3.3	4.069	0.076	2.56
Fine	1562462	3.44	0	0.078	0

Tab. 3. Geometric parameters of propeller model

Geometric parameters	**Value**
Number of rotor blade	4
Rotor radius *R* (m)	0.82
Blade chord (m)	0.065
Pitch angel (°)	8°
Angular speed (rpm)	900
Blade airfoil	NACA0414
Blade airfoil camber (%)	0.5%
Blade airfoil thickness (%)	14.9%
Blade twist (°)	0°

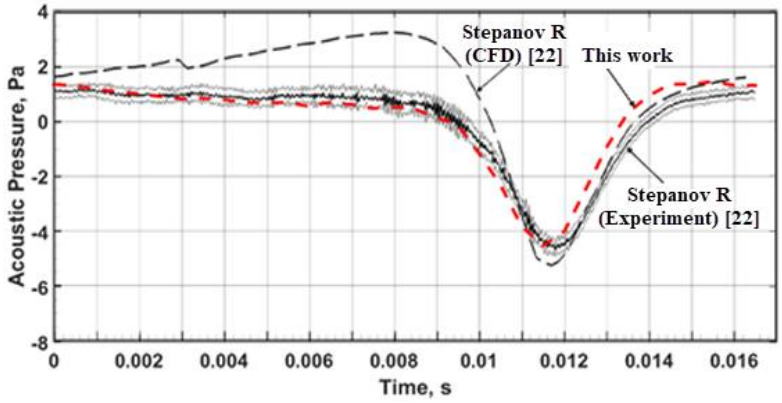

Fig. 5. Verifying acoustic simulation results [21].

3. Results and discussions

Simulations were carried out in transient mode with a time step (*dt*) of 0.0001 s. After 1200 iterations over a time of 0.3 s, the propeller completed 25 rotations, with the convergence image and the distribution of the y+ index on the propeller surface shown in Fig. 6 and Fig. 7. The y+ value is a crucial parameter in CFD simulations, particularly in grid generation and assessing the accuracy of turbulence models in near-wall regions. In this study, the y+ value falls within the range of $1 < y+ < 5$, meaning that the grid points are located within the viscous sublayer, indicating good grid quality. This region is where the flow velocity varies linearly with the distance to the wall, commonly used in direct modeling or near-wall turbulence models (Fig. 7).

The images of the airflow motion and velocity distribution on the vertical plane for the independent propeller model (IndePro) and the Propeller - Boundary surface model (Pro - BF) with different *h* values are shown in Fig. 8. The simulation images clearly show the difference in airflow motion caused by the IndePro and the Pro - BF model. Without the obstruction of the boundary surface, the airflow beneath the independent propeller is strongly pushed downward and moves away from the propeller surface. With the boundary surface, the airflow is blocked and pushed to the sides, forming vortices at the two edges of the boundary surface. Depending on the distance *h*, the vortices have different sizes, and the induced velocity values of the air molecules in the vortices also vary. When the propeller is near the boundary surface ($h = 0.5R$), the vortices on both sides of the boundary surface edge and at the propeller blade tips are most clearly observed. The induction effect of the vortices and the boundary surface itself on the propeller surfaces increases the pressure on the lower surface of the propeller blades, thereby increasing the propeller's thrust (Fig. 9).

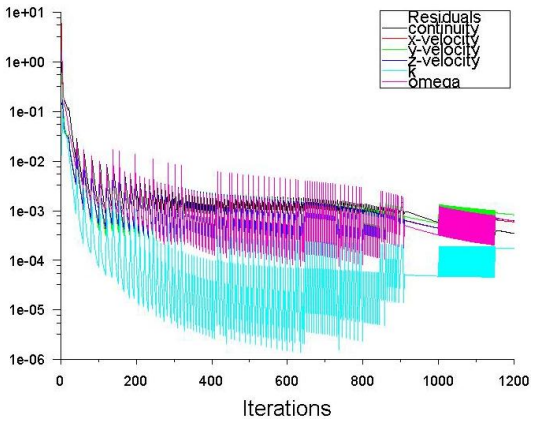

Fig. 6. Convergence graph after 1200 iterations.

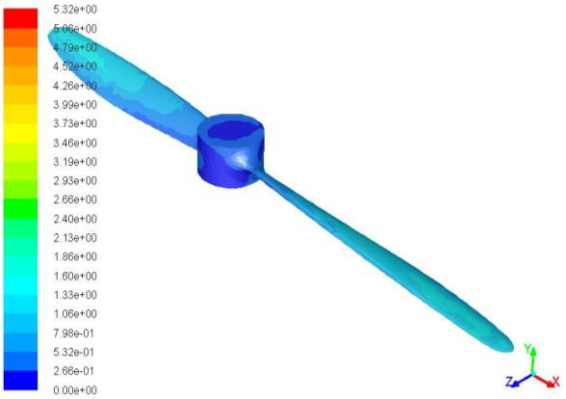

Fig. 7. Y+ index on the surface of the propeller.

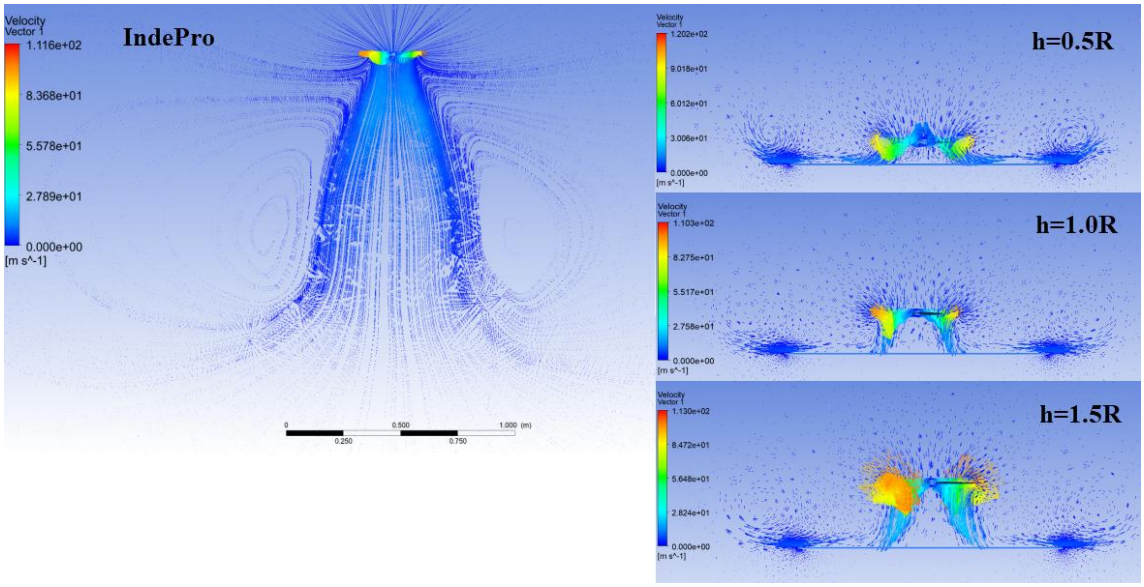

Fig. 8. Vortex formation by the IndePro and Pro - BF model at Ω = 7000 rpm with different h values.

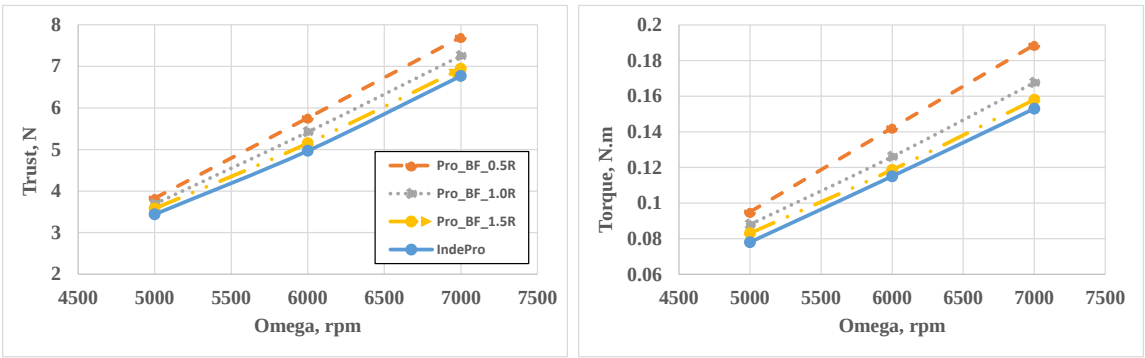

Fig. 9. Thrust and torque of the propeller with different Ω and h values.

The lift and torque generated by the propeller under different operating conditions are shown in Fig. 9. Here, the rotational speed of the propeller takes on values of 5000 rpm, 6000 rpm, and 7000 rpm, and the distances from the propeller to the ground plane are 0.5*R*, 1.0*R*, and 1.5*R*, respectively (Fig. 2). The calculation results indicate that in all different cases of h, the higher the rotational speed, the greater the thrust and required torque produced by the propeller. Additionally, the closer the propeller is to the boundary surface, the greater the effect of the ground effect, resulting in higher lift values.

At the microphone positions 1, 2, and 3 (Fig. 3), the authors examined the propagation of noise generated by the propeller to the microphones in two cases: The first case is when the boundary surface can completely absorb and not reflect sound (BF non-reflec). The sound received at microphones 1, 2, and 3 consists only of direct sound transmission from the propeller (direct sound). The second case is when the boundary surface does not absorb and completely reflects sound (BF reflec). In this case, the sound received at microphones 1, 2, and 3 includes two components: direct sound from the propeller and indirect sound from the propeller that is reflected by the boundary surface to the microphones.

The variations in sound pressure level (SPL) obtained at microphones 1, 2, and 3 are shown in Fig. 10. The results indicate that in the case where the boundary surface does not absorb and completely reflect sound, the SPL values recorded at all three microphones are higher compared to the non-reflective case and the independent propeller case. The non-reflective boundary surface case shows SPL values that do not differ significantly from the independent propeller case.

Figures 11 and 12 show the overall sound pressure level (OASPL, calculated according to expression (5)) caused by the independent propeller (IndePro) and the propeller with boundary surface (Pro_BF) at different distances h and rotation speeds Ω. In this case, the boundary surface is considered to completely reflect sound. The variations in the graphs indicate that the propeller operating in ground effect, the closer it is to the boundary surface, generates more noise. Comparing the overall sound pressure levels recorded at microphones 1, 2, and 3 shows that the noise at mic 2 is always higher than at mics 1 and 3. However, when changing the distance h, the variation in the overall sound pressure level at mic 2 is not significant, whereas at mics 1 and 3, there is a considerable increase (Fig. 11). This could be due to the influence of vortices formed

when the propeller hovers near the boundary surface, which tends to move vertically and affects the sound pressure levels at mics 1 and 3 more than at mic 2.

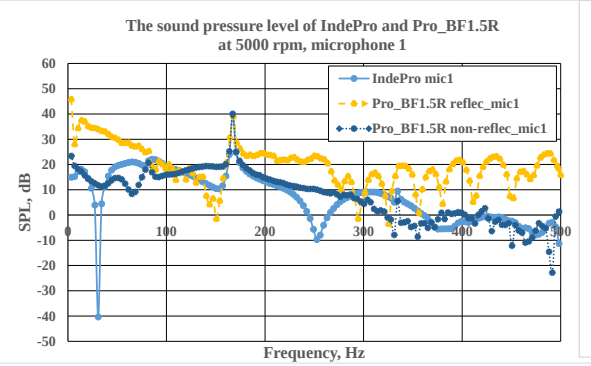

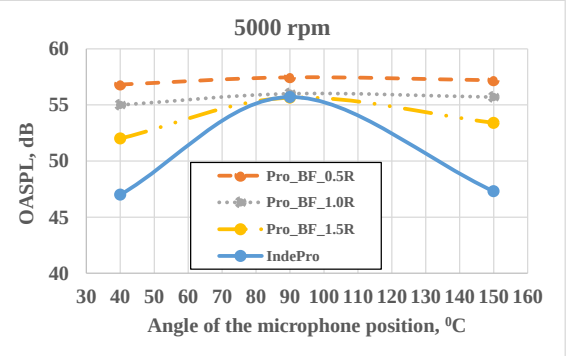

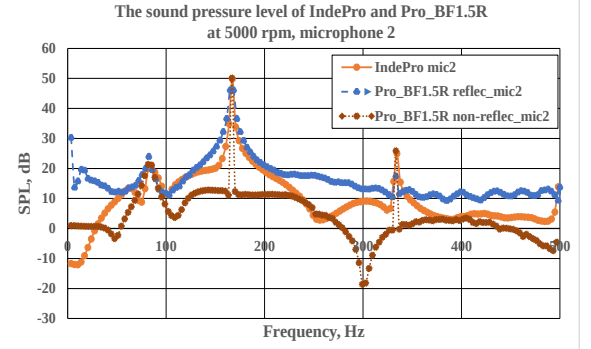

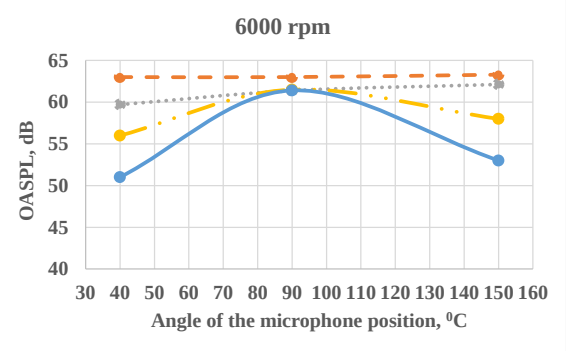

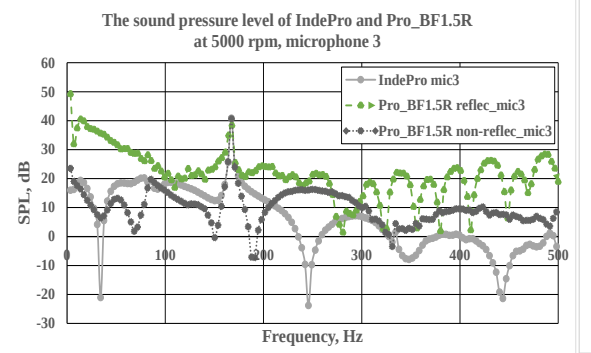

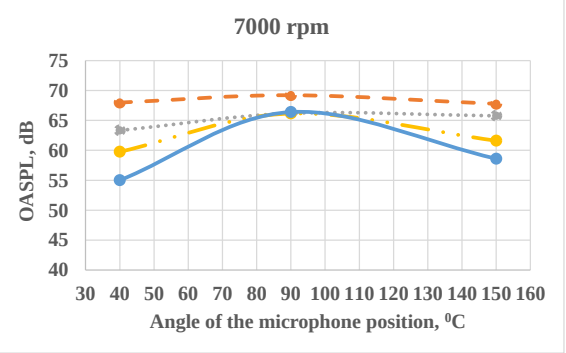

Fig. 10. Variation of the sound pressure level with frequency obtained at microphones 1, 2, 3 by IndePro and Pro_BF with h = 1.5R, Ω = 5000 rpm.

Fig. 11. Overall sound pressure level obtained at microphones 1, 2, 3 by IndePro and Pro_BF at different distances h and rotation speeds Ω.

Figure 12 shows that increasing the rotation speed of the propeller significantly increases the noise recorded at mics 1, 2, and 3.

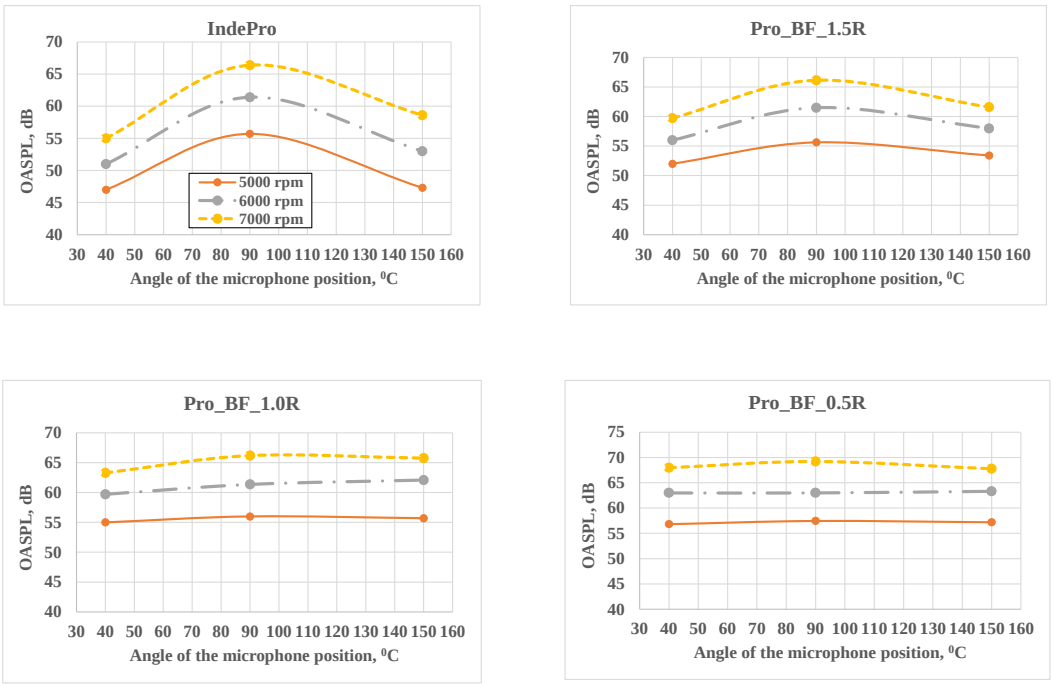

Fig. 12. Overall sound pressure level caused by IndePro and Pro_BF at microphones 1, 2, 3.

4. Conclusions

This article presents an approach using the RANS method combined with CFD techniques to simulate the aerodynamic characteristics of a propeller considering the influence of a boundary surface. It also employs an acoustic analogy method based on the Farassat 1A formula, derived from the FW-H equation, integrated into Ansys Fluent software to calculate the noise generated by the propeller and the boundary surface at different positions. The study results indicate that the boundary surface significantly affects the aerodynamic and acoustic characteristics of the propeller, especially when the propeller operates close to the boundary surface. The reflective or absorptive properties of the boundary surface also clearly impact the sound pressure levels recorded at the measurement locations. Additionally, specific operating conditions of the propeller, such as rotation speed and flight mode, have a noticeable effect on its aerodynamic and acoustic properties. The findings in this paper serve as a valuable reference for optimizing the design of propellers for aviation equipment, finding solutions to reduce propeller noise, and studying sound-absorbing materials. In the following studies, the authors aim to study the boundary surface shape's influence on the propeller's aerodynamic noise characteristics.

Acknowledgement

This article is a product of the regular project at Le Quy Don Technical University level, code number 24.1.31.

References

[1] B. M. Efimtsov and L. A. Lazarev, "Evaluation of the effect of stopping selected frames on noise in the cabin of a propeller airplane", *Acoustical Physics*, Vol. 61, No. 4, pp. 466-475, 2015. DOI: 10.1134/S106377101504003X

[2] Y. D. Khaletskiy and Y. S. Pochkin, "Fan noise reduction of an aircraft engine by inclining the outlet guide vanes", *Acoustical Physics*, Vol. 61, No. 1, pp. 101-108, 2015. DOI: 10.1134/S1063771014060098

[3] I. V. Belyaev, "The effect of an aircraft's boundary layer on propeller noise", *Acoustical Physics*, Vol. 58, No. 4, pp. 387-395, 2012. DOI: 10.1134/S1063771012040045

[4] D. Miljković, "Methods for attenuation of unmanned aerial vehicle noise", *41st International Convention on Information and Communication Technology, Electronics and Microelectronics (MIPRO)*, Opatija, Croatia, pp. 0914-0919, IEEE, 2018. DOI: 10.23919/MIPRO.2018.8400169

[5] A. Mehrabi and A. R. Davari, "Outwash flow measurement around the subscale tandem rotor in ground effect", *Engineering Science and Technology, an International Journal*, Vol. 23, No. 6, pp. 1374-1384, 2020. DOI: 10.1016/j.jestch.2020.08.016

[6] Y. Luo, T. Ai, Y. He *et al.*, "Numerical investigation on unsteady characteristics of ducted fans in ground effect", *Chinese Journal of Aeronautics*, Vol. 36, Iss. 9, pp. 79-95, 2023. DOI: 10.1016/j.cja.2023.04.004

[7] F. Farassat and G. P. Succi, "A review of propeller discrete frequency noise prediction technology with emphasis on two current methods for time domain calculations", *Journal of Sound and Vibration*, Vol. 71, No. 3, pp. 399-419, 1980.

[8] F. Farassat, *Derivation of Formulations 1 and 1A of Farassat*. No. L-19318, NASA/TM, 2007.

[9] A. Najafi-Yazdi, G. A. Brès, and L. Mongeau, "An acoustic analogy formulation for moving sources in uniformly moving media", *Proceedings of the Royal Society A: Mathematical, Physical and Engineering Sciences*, Vol. 467, No. 2125, pp. 144-165, 2011. DOI: 10.1098/rspa.2010.0172

[10] J. E. Ffowcs Williams and D. L. Hawkings, "Sound generation by turbulence and surfaces in arbitrary motion", *Philosophical Transactions for the Royal Society of London. Series A, Mathematical, Physical and Engineering Sciences*, Vol. 264, Iss. 1151, pp. 321-342, 1969. DOI: 10.1098/rsta.1969.0031

[11] P. T. Đồng, N. A. Tuấn, Đ. N. Thanh và P. V. Uy, "Xây dựng mô hình tính toán các đặc trưng khí động của cánh quay trực thăng", *Tuyển tập Công trình Hội nghị khoa học các nhà nghiên cứu trẻ lần thứ XII - năm 2017/Tạp chí Khoa học và Kỹ thuật* - ISSN 1859-0209, Số 185, tr. 70-79, 2017.

[12] P. T. Đồng, N. A. Tuấn, Đ. N. Thanh và P. V. Uy, "Nghiên cứu ảnh hưởng của địa hình đến đặc trưng khí động của trực thăng khi hạ cánh", *Tuyển tập Công trình Hội nghị khoa học các nhà nghiên cứu trẻ lần thứ XIV - năm 2019/Tạp chí Khoa học và Kỹ thuật* - ISSN 1859-0209, Số 197, tr. 71-79, 2019. DOI: 10.56651/lqdtu.jst.v14.n02.434

[13] Q. Q. Le, T. D. Pham, Q. T. Vu, and A. T. Nguyen, "Building and verifying a tool for calculating the aerodynamic noise of helicopter rotors", *Journal of Science and Technique* - ISSN 1859-0209, Vol. 17, No. 05, pp. 58-69, 2022. DOI: 10.56651/lqdtu.jst.v17.n05.530

[14] Q. Liu, D. Qi, and Y. Mao, "Numerical calculation of centrifugal fan noise", *Proceedings of the Institution of Mechanical Engineers, Part C: Journal of Mechanical Engineering Science*, Vol. 220, No. 8, pp. 1167-1177, 2006. DOI: 10.1243/09544062JMES211

[15] L. Yang, J. Huang, M. Yi, C. Zhang, and Q. Xiao, "A numerical study of the effects of design parameters on the acoustics noise of a high efficiency propeller", *Acoustical physics*, Vol. 63, Iss. 6, pp. 699-710, 2017. DOI: 10.1134/S1063771017060033

[16] Z. H. Han, W. P. Song, and Z. D. Qiao, "Aeroacoustic calculation for helicopter rotor in hover and in forward flight based on FW-H equation", *Acta Aeronautica et Astronautica Sinica*, Vol. 24, No. 5, pp. 400-404, 2003. https://api.semanticscholar.org/CorpusID: 124461936.

[17] F. Fan, Y. J. Shi, and G. H. Xu, "Computational research on aerodynamic and aeroacoustic characteristics of scissors tail-rotor in hover", *Acta Aeronautica et Astronautica Sinica*, Vol. 34, No. 9, pp. 2100-2109, 2013. DOI: 10.7527/S1000-6893.2013.0111

[18] B. B. Hu, H. O. Yang, Y. D. Wu *et al.*, "Numerical prediction of the interaction noise radiated from an axial fan", *Applied Acoustics*, Vol. 74, No. 4, pp. 544-552, 2013. DOI: 10.1016/j.apacoust.2012.09.009

[19] W. H. Lam, G. A. Hamill, and D. J. Robinson, "Initial wash profiles from a ship propeller using CFD method", *Ocean Engineering*, Vol. 72, pp. 257-266, 2013. DOI: 10.1016/j.oceaneng.2013.07.010

[20] K. J. Lee, J. H. Bae, H. T. Kim, and T. Hoshino, "A performance study on the energy recovering turbine behind a marine propeller", *Ocean Engineering*, Vol. 91, No. 152-158, 2014. DOI: 10.1016/j.oceaneng.2014.09.004

[21] L. Q. Quyền, P. T. Đồng, V. Q. Trụ và N. A. Tuấn, "Nghiên cứu mô phỏng số tiếng ồn khí động của cánh quay trực thăng bằng CFD", *Tuyển tập Công trình Hội nghị khoa học các nhà nghiên cứu trẻ lần thứ XVII - năm 2022*, Nxb Quân đội nhân dân, ISBN: 978-604-51-824-7-5, Hà Nội, 2022.

[22] R. Stepanov, V. Pakhov, A. Bozhenko, and A. Batrakov, "Experimental and numerical study of rotor aeroacoustics", *International Journal of Aeroacoustics*, Vol. 16, No. 6, pp. 460-475, 2017. DOI: 10.1177/1475472X177304

NGHIÊN CỨU XÁC ĐỊNH TIẾNG ỒN KHÍ ĐỘNG CỦA CÁNH QUAY XÉT ĐẾN ẢNH HƯỞNG CỦA MẶT GIỚI HẠN BẰNG PHƯƠNG PHÁP CFD

Phạm Thành Đồng[1], Lê Quang Quyền[1], Đặng Ngọc Thanh[1], Vũ Quốc Trụ[1]

[1]*Khoa Hàng không vũ trụ, Trường Đại học Kỹ thuật Lê Quý Đôn*

Tóm tắt: Trong bài báo này, các đặc trưng khí động học và âm học của mô hình cánh quay độc lập và mô hình cánh quay - mặt giới hạn được tập trung nghiên cứu. Quá trình phân tích khí động học được thực hiện bằng phương pháp RANS kết hợp với kỹ thuật CFD để mô phỏng trường dòng chảy và dòng nhiễu sau cánh quay, đồng thời xác định các hệ số khí động cơ bản của một cánh quay. Áp suất trên bề mặt cánh quay và mặt giới hạn trong bài toán khí động đóng vai trò làm đầu vào của các tính toán tiếng ồn. Bài báo sử dụng phương pháp tương tự âm học, dựa trên công thức Farassat 1A có nguồn gốc từ phương trình FW-H, để tính toán sự lan truyền của tiếng ồn từ các bề mặt cánh quay và mặt giới hạn đến các vị trí khác nhau cho trước (các micro thu). Trên cơ sở các kết quả nghiên cứu, nhóm tác giả rút ra một số kết luận có ý nghĩa.

Từ khóa*: Cánh quay; đặc tính khí động; tiếng ồn khí động; Farassat 1A.*

Received: 18/07/2024; Revised: 26/08/2024; Accepted for publication: 21/11/2024

❑